iScience

CellPress
OPEN ACCESS

Article

Translational modulator ISRIB alleviates synaptic and behavioral phenotypes in Fragile X syndrome

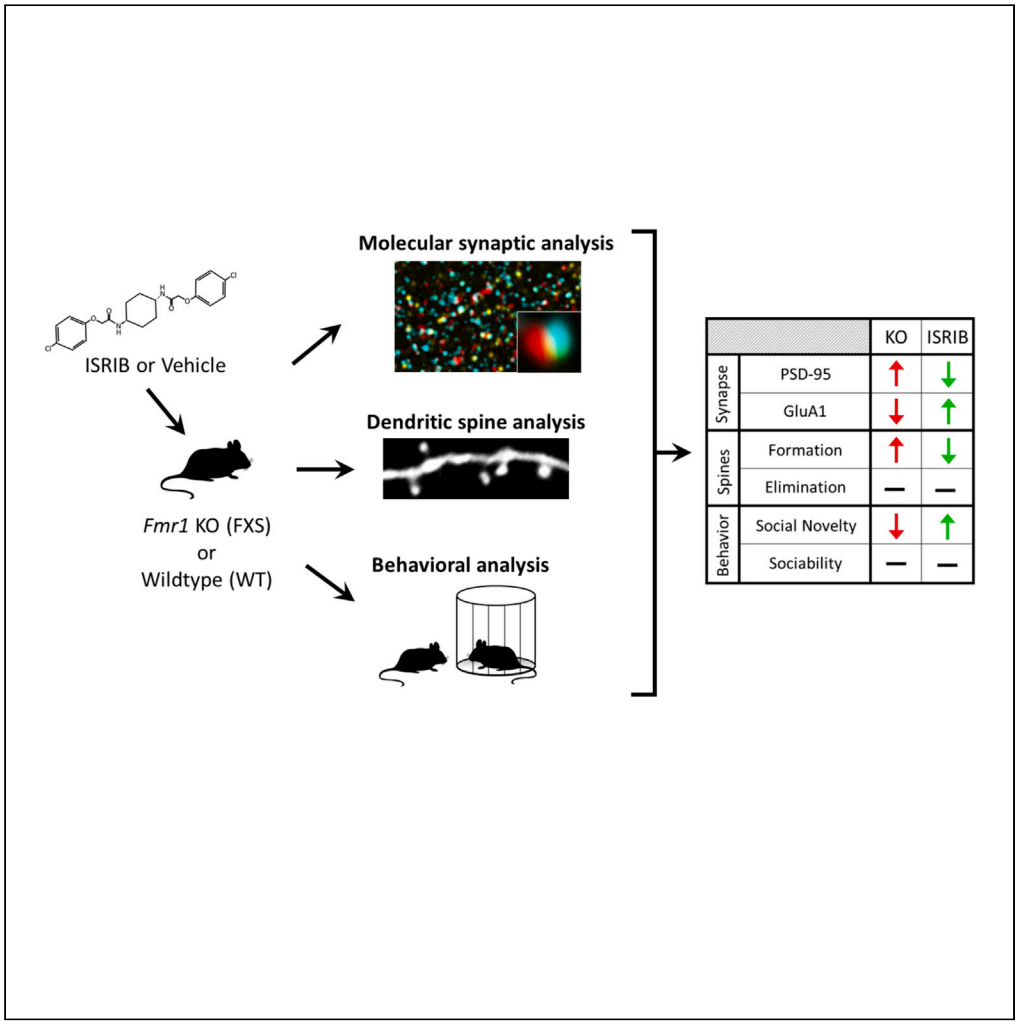

Rochelle L. Coulson, Valentina Frattini, Caitlin E. Moyer, ..., Philippe Mourrain, Yi Zuo, Gordon X. Wang

yizuo@ucsc.edu (Y.Z.)
gordon.wang@stanford.edu (G.X.W.)

Highlights

Elevated PSD-95 but not GluA1 leads to excess immature spines in *Fmr1* KO mice

Translational regulator ISRIB normalizes synaptic proteins and spine turnover

The effect of ISRIB at the synapse is independent of global protein synthesis

ISRIB rescues social recognition deficits in *Fmr1* KO mice

Coulson et al., iScience *27*, 109259
April 19, 2024
https://doi.org/10.1016/j.isci.2024.109259

iScience

CellPress
OPEN ACCESS

Article

Translational modulator ISRIB alleviates synaptic and behavioral phenotypes in Fragile X syndrome

Rochelle L. Coulson,[1] Valentina Frattini,[1] Caitlin E. Moyer,[2] Jennifer Hodges,[3] Peter Walter,[4,5,8] Philippe Mourrain,[1,6] Yi Zuo,[3,*] and Gordon X. Wang[1,7,9,*]

SUMMARY

Fragile X syndrome (FXS) is caused by the loss of fragile X messenger ribonucleoprotein (FMRP), a translational regulator that binds the transcripts of proteins involved in synaptic function and plasticity. Dysregulated protein synthesis is a central effect of FMRP loss, however, direct translational modulation has not been leveraged in the treatment of FXS. Thus, we examined the effect of the translational modulator integrated stress response inhibitor (ISRIB) in treating synaptic and behavioral symptoms of FXS. We show that FMRP loss dysregulates synaptic protein abundance, stabilizing dendritic spines through increased PSD-95 levels while preventing spine maturation through reduced glutamate receptor accumulation, thus leading to the formation of dense, immature dendritic spines, characteristic of FXS patients and *Fmr1* knockout (KO) mice. ISRIB rescues these deficits and improves social recognition in *Fmr1* KO mice. These findings highlight the therapeutic potential of targeting core translational mechanisms in FXS and neurodevelopmental disorders more broadly.

INTRODUCTION

Neurodevelopmental disorders such as Autism spectrum disorder (ASD) and Fragile X syndrome (FXS) are associated with social and cognitive deficits, and are increasingly prevalent, with an estimated 1 in 54 children diagnosed with ASD in the United States.[1] FXS is the most common monogenic cause of inherited intellectual disability and ASD[2] and is characterized by many common autistic traits including cognitive dysfunction, social phobia, stereotyped behavior, hyperactivity, and hypersensitivity to sensory stimuli.[3,4] Due to the well-defined genetic etiology of FXS, pharmacological targeting of abnormal cellular and molecular pathways is possible and holds promise for the development of therapies for the treatment of neurodevelopmental disorders and ASD in general.[5]

In humans, FXS is most often caused by the expansion of a CGG trinucleotide beyond 200 repeats within the 5′-untranslated region (UTR) of the fragile X messenger ribonucleoprotein 1 gene (*FMR1*). This inhibits *FMR1* transcription and the production of the highly conserved fragile X messenger ribonucleoprotein (FMRP).[6] FMRP is an RNA-binding protein that regulates the translation of approximately 4% of all transcripts in the brain.[7] Many of these transcripts encode proteins that regulate synaptic function and plasticity, such as PSD-95, GluA1, GluA2, ARC, and MAP1B.[7–16] Protein translation, especially in the highly active awake brain, is extremely metabolically demanding. Behaviors such as socialization and learning induce significant metabolic load on a cellular and synaptic level in neurons.[17,18] Translation dependent mechanisms regulating this metabolic response are critical for proper synaptic network function and plasticity.[19]

Altered brain metabolism due to dysregulated protein synthesis in the absence of FMRP[20,21] suggests that drugs targeting translational regulation of stress pathways may alleviate FXS synaptic deficits and improve behavioral outcomes. One such drug is the small molecule integrated stress response inhibitor (ISRIB). ISRIB modulates translation in a context-specific manner, acting on a specific set of mRNAs that are preferentially translated under stress conditions, rather than altering bulk translation throughout the cell, and impacting translational processes involved in synaptic plasticity.[22–26] Cell-type-specific dysregulation of the integrated stress response has been shown in *Fmr1* KO excitatory neurons,[27] suggesting that context-specific local translational programs in neuronal synapses represent a key switching mechanism that regulates plasticity. In a normal neuron, FMRP regulates translation at the synapse.[11] In the absence of FMRP, ISRIB may compensate for some

[1]Department of Psychiatry and Behavioral Sciences, Stanford University, Stanford, CA 94305, USA
[2]National Institute on Drug Abuse, National Institutes of Health, Bethesda, MD 20892, USA
[3]Department of Molecular, Cell and Developmental Biology, University of California Santa Cruz, Santa Cruz, CA 95064, USA
[4]Howard Hughes Medical Institute, University of California San Francisco, San Francisco, CA 94143, USA
[5]Department of Biochemistry and Biophysics, University of California San Francisco, San Francisco, CA 94143, USA
[6]INSERM 1024, Ecole Normale Supérieure, Paris, France
[7]Wu Tsai Neuroscience Institute, Stanford University, Stanford, CA 94305, USA
[8]Present address: Altos Labs, Inc., Redwood City, CA 94065, USA
[9]Lead contact
*Correspondence: yizuo@ucsc.edu (Y.Z.), gordon.wang@stanford.edu (G.X.W.)
https://doi.org/10.1016/j.isci.2024.109259

of the functions of FMRP as a translational regulator of plasticity and function at neuronal synapses. The efficacy of ISRIB in the absence of FMRP is unknown, thus we examined the effects of ISRIB treatment by characterizing the synaptic mechanisms underlying ISRIB activity in the *Fmr1* KO mouse model. Specifically, we sought to determine if ISRIB could compensate for the loss of translational regulation by FMRP and whether restoring synaptic protein expression could rescue behavioral outcomes in FXS.

In this study we examine the effects of FMRP deficiency at the molecular, synaptic, and behavioral levels to characterize the mechanisms underlying the cognitive impairment observed in FXS. We used synapse-scale proteomic imaging[28–30] and *in vivo* dendritic spine imaging[31] to identify previously undescribed molecular and structural synaptic changes caused by the loss of FMRP and their response to ISRIB. We further demonstrate that molecular synaptic rescue corresponds with a normalization of dendritic spine dynamics and social recognition. In summary, we show that the loss of FMRP, and the accompanying translational modulation at the synapse, induces a heterogeneous synaptic response and dysregulated protein accumulation in synapses along with social deficits in *Fmr1* KO mice, which can be rescued through the restoration of synaptic protein accumulation by ISRIB.

RESULTS

Fmr1 KO mice exhibit increased PSD-95 accumulation in a subset of synapses

In humans and mouse models, FXS is associated with increased spine density and immature spine morphology.[32,33] These spine changes are hypothesized to be physical manifestations of synaptic network alterations.[34] However, the exact nature of synaptic protein changes in FXS has been difficult to assess, especially on a synapse-specific, population level. An important synaptic protein for studying the mechanism of excitatory synaptic network changes in FXS is PSD-95. PSD-95 plays a key role in organizing synaptic structure[35,36] and activity-dependent stabilization of spines and synaptic strengthening.[37] Further, PSD-95 mRNA stability and translation are regulated by FMRP.[16,38,39] We examined the effect of FMRP deficiency on PSD-95 abundance in individual synapses using a super-resolution, single synapse analysis method that combines array tomography (AT) with a computational synapse classification algorithm developed in our lab[29,30] to identify changes in specific molecularly defined synaptic populations. This enables us to analyze all synapses of a specific class, e.g., vesicular glutamate transporter 1 (VGluT1)-expressing excitatory, cortical-cortical synapses, with single synapse resolution, and metrics across entire populations.[29] Thus, we were able to examine the unique effects of FMRP deficiency within specific synapse populations, while still maintaining our ability to resolve individual synaptic protein changes. We measured PSD-95 volume in cortical-cortical excitatory synapses. PSD-95 volume is demonstrated to be an excellent indicator of synapse size and maturity by electron microscopy (EM).[40] PSD-95 volume is dependent on both abundance and localization at the synapse, thus changes in anchoring factors such as α-actinin may influence PSD-95 accumulation at the synapse,[41] however, compared among several postsynaptic scaffolds, PSD-95 remains stable upon F-actin disruption.[42] While PSD-95 volume alone is not an absolute measure of synapse size, it plays a role in the anchoring of other postsynaptic factors critical for spine stabilization and is thus an informative measure of spine maturation.[35] Cumulative distribution plots of wild type (WT) and *Fmr1* KO PSD-95 volume size indicate a significant increase ($p < 2.2 \times 10^{-16}$, Kolmogorov-Smirnov) in synapse size in layer 1 cortical-cortical synapses of the motor cortex (Figure 1A). This shift is easily visualized in a density plot (Figure 1B), where the WT distribution of PSD-95 volume across the entire synapse population is more skewed toward smaller volumes than the *Fmr1* KO synapse population. This is further reflected in a 33% increase in median PSD-95 levels in vehicle-treated *Fmr1* KO mice compared to their vehicle-treated WT counterparts ($p < 2.2 \times 10^{-16}$, Mann-Whitney U) (Figures 1A–1C; Table S1). In layer 2/3, the change in PSD-95 levels is minimal, with only a 3.8% increase in median volume observed in *Fmr1* KO mice (Figure S1; Table S1). Elevated PSD-95 levels in layer 1 *Fmr1* KO mouse synapses are reduced by ISRIB treatment, bringing them closer to WT levels (Figures 1A–1C). This normalization of the distribution of PSD-95 suggests that ISRIB partially compensates for the loss of FMRP in maintaining balanced protein abundance at the synapse.

ISRIB increases GluA1 levels at the postsynaptic terminal in *Fmr1* KO mice

PSD-95 is important for the activity-dependent stabilization of spines and synaptic maturation.[37] The increase in volume of PSD-95 in layer 1 suggests a possible mechanism for the elevated stabilization of spines leading to higher spine and synapse density,[29,43,44] but it does not provide a rationale for the immature morphology of the spines. A possible explanation is that loss of synaptic protein regulation in the absence of FMRP increases PSD-95 and spine stabilization but perturbs the accompanying process of spine and synapse maturation. One such maturation process proceeds through AMPA receptor subunit GluA1-mediated plasticity.[37,45–47] PSD-95 accumulation is coupled with the clustering of GluA1 at the postsynaptic terminal.[45] The loss of FMRP-mediated translational regulation leads to reduction of membrane surface AMPA receptors localized at dendritic spines.[48] We hypothesized that ISRIB could compensate for this loss, normalizing glutamate receptor-mediated maturation of the synapse. Therefore, we measured GluA1 protein levels at molecularly classified excitatory synapses in vehicle- and ISRIB-treated WT and *Fmr1* KO mice. To clearly determine the effect of ISRIB at the synapse, we calculated the ratio of GluA1 integrated intensity in excitatory synapses with or without ISRIB treatment (Figures 1D and 1E; Figure S2; Table S2). A ratio of one indicates no effect of treatment on GluA1 abundance, with values greater than one indicating an increase in protein abundance with ISRIB treatment, and values less than one representing a decrease in abundance. ISRIB treatment significantly increased postsynaptic GluA1 levels in *Fmr1* KO mice compared to WT in layers 1 and 2/3 of the cortex (Figure 1D) ($p = 0.031$ (L1), $p = 0.016$ (L2/3), Mann-Whitney U). We demonstrated that synaptic PSD-95 is elevated in *Fmr1* KO synapses which, without a concomitant increase in GluA1, may impede the normal process of synaptic strengthening and maturation. Furthermore, these FXS-specific synaptic protein changes can be normalized by ISRIB.

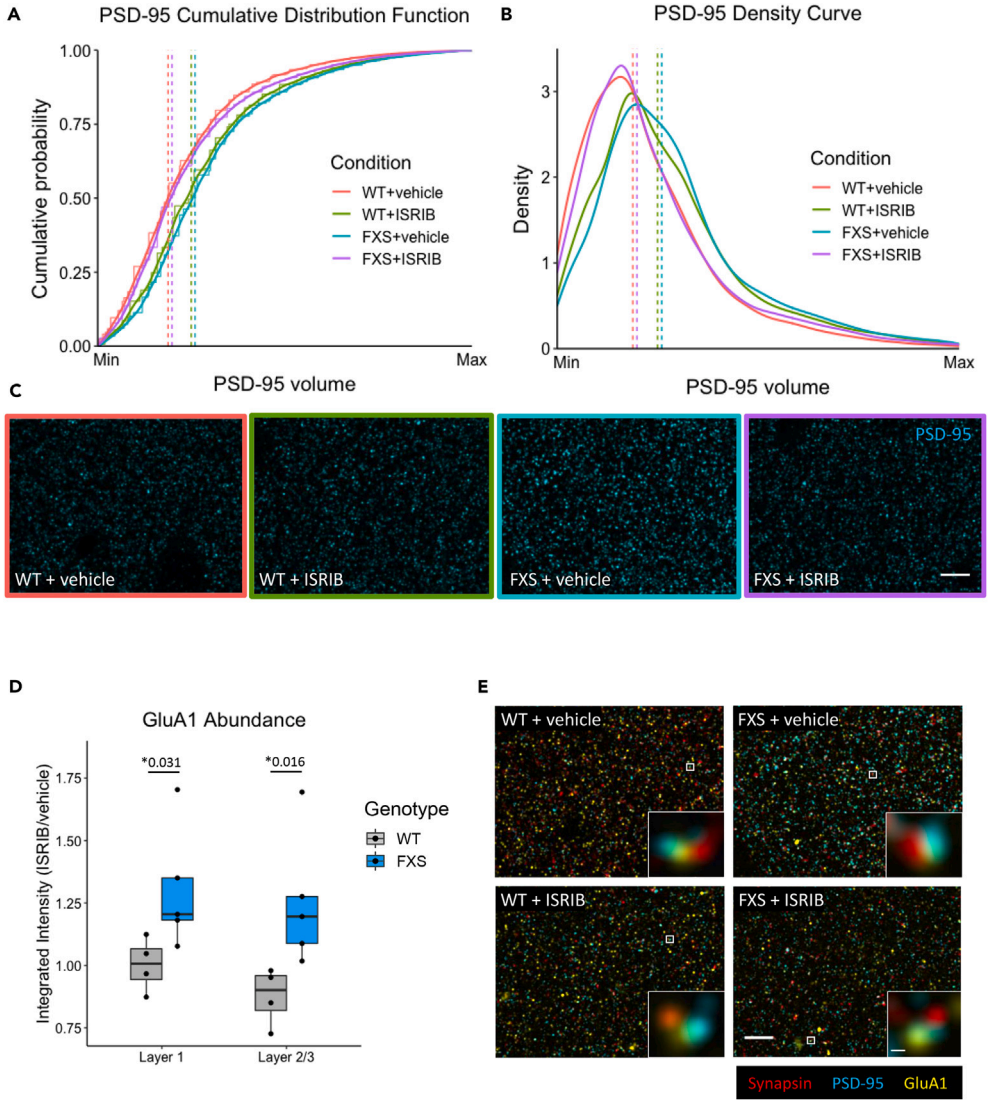

Figure 1. Array tomography (AT) analysis of PSD-95 and GluA1 abundance

(A) Cumulative distribution function (CDF) of PSD-95 size. PSD-95 volume was normalized to the maximum PSD-95 volume observed per mouse to normalize for experimental variability and the cumulative probability was plotted across the range of PSD-95 volumes. The raw CDF is shown as steps with the smoothed CDF overlayed for each condition. Vertical dashed lines indicate the median PSD-95 volume for each condition. Median = 0.21 WT + vehicle, 0.27 WT + ISRIB, 0.28 FXS + vehicle, and 0.22 FXS + ISRIB. The distribution of PSD-95 among all synapses is altered in FXS layer 1 cortex, with fewer small PSD-95 synapses and a shift toward larger PSD-95 synapses. This shift results in a significantly altered PSD-95 synapse distribution (WT + vehicle vs. FXS + vehicle, Kolmogorov-Smirnov, $p < 2.2x10^{-16}$) and a 33% increase in median PSD-95 size (WT + vehicle vs. FXS + vehicle, Mann-Whitney U, $p < 2.2x10^{-16}$), which is decreased upon ISRIB treatment (FXS + vehicle vs. FXS + ISRIB, Kolmogorov-Smirnov and Mann-Whitney U, $p < 2.2x10^{-16}$).

(B) PSD-95 size shown as a density plot. Loss of small PSD-95 synapses is accompanied by a gain of larger PSD-95 synapses. Medians are shown as vertical dashed lines (values as stated in A).

(C) Representative AT images for PSD-95 are shown for each condition. Imaging was performed blind to genotype and condition and images were taken at the same exposure. Images are a max projection throughout the depth of tissue. Scale bar: 5 μm. FXS = *Fmr1* KO. n = 4 WT + vehicle (49,631 synapses), 4 WT + ISRIB (34,061 synapses), 5 FXS + vehicle (49,375 synapses), and 5 FXS + ISRIB (49,350 synapses).

(D) Integrated intensity for GluA1 was normalized for exposure and is the weighted average of VGluT1 and VGluT2 synapses. Tissues were processed and imaged in pairs and the ratio of integrated intensity for ISRIB/vehicle-treated mice was plotted. A ratio of one indicates no drug effect on abundance, with values above one indicating an increase in abundance with ISRIB treatment and values less than one indicating a decrease. ISRIB significantly increases GluA1 abundance in FXS synapses in both layers 1 (WT vs. FXS, p = 0.031) and 2/3 (WT vs. FXS, p = 0.016).

(E) Representative AT images for layer 1 synapses in each condition including both a wide field view (scale bar: 5 μm) and individual synapses (scale bar: 200 nm). Individual synapses show Synapsin (red), PSD-95 (cyan), and postsynaptically localized GluA1 (yellow). Images are a max projection throughout the depth of tissue. Significance was calculated by Mann-Whitney U test. FXS = *Fmr1* KO. n = 4 WT + vehicle, 4 WT + ISRIB, 5 FXS + vehicle, and 5 FXS + ISRIB. See also Figures S1, S2 and Tables S1, S2.

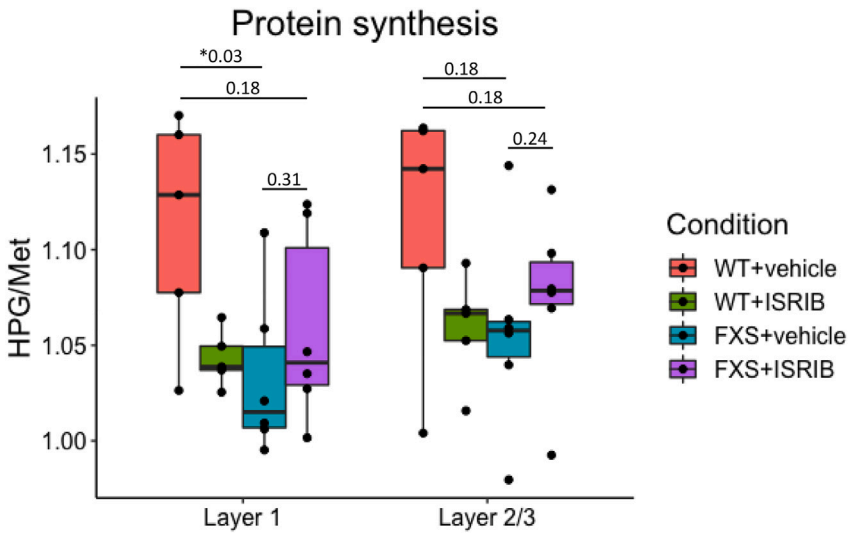

Figure 2. Global protein synthesis in *Fmr1* KO (FXS) and WT motor cortex

Protein synthesis was measured by FUNCAT in acute brain slices treated with ISRIB or a vehicle control. The noncanonical amino acid HPG is incorporated into newly synthesized proteins and methionine (Met) is incorporated as a negative control. Protein synthesis is significantly lower in layer 1 of the motor cortex in FXS mice compared to WT mice (WT + vehicle vs. FXS + vehicle, p = 0.03). Global protein synthesis levels are not restored by ISRIB treatment (FXS + vehicle vs. FXS + ISRIB, p = 0.31). Significance was measured by Mann-Whitney U test. FXS = *Fmr1* KO. n = 5 WT + vehicle, 5 WT + ISRIB, 5 FXS + vehicle, 5 FXS + ISRIB.

Reduced global protein synthesis in *Fmr1* KO is not rescued by ISRIB

FMRP is a bidirectional regulator of translation, acting in a context-specific manner to modulate protein synthesis at the synapse. Factors such as transcript length, brain region, local cellular compartmentalization, developmental stage, and activity-dependent signaling all contribute to the functional output of FMRP regulation.[49] Thus, translational dysregulation in the absence of FMRP is more nuanced than previously considered, often resulting in a skewed translational profile, with increases, decreases, and no net changes in bulk protein abundance reported depending on the combinatorial impact of these factors.[50–57] More recently, loss of FMRP has been shown to favor the translation of short ribosomal transcripts at the expense of long transcripts, many of which localize and function at the synapse.[58,59] To complement our synaptic approach, we examined total cellular *de novo* protein synthesis by fluorescent noncanonical amino acid tagging (FUNCAT) in WT and *Fmr1* KO acute brain slices treated with ISRIB or a vehicle control. Protein synthesis was significantly reduced in *Fmr1* KO compared to WT in layer 1 of the motor cortex (Figure 2) (p = 0.03, Mann-Whitney U). ISRIB does not restore translational regulation at the cellular level (*Fmr1* KO + vehicle vs. *Fmr1* KO + ISRIB, p = 0.31, Mann-Whitney U). A similar pattern was observed in layer 2/3, but changes did not reach significance. Differences in protein synthesis and abundance at the cellular and synaptic levels demonstrate the various mechanisms of bulk and local translation regulation by FMRP. Additionally, this highlights the specificity of ISRIB, which preferentially acts on stress-mediated translational pathways. These differences also suggest that ISRIB plays a role in regulating synaptic protein abundance in FXS that is distinct from global cellular translation.

ISRIB rescues abnormal spine dynamics in the cortex

The accumulation of PSD-95 and GluA1 in the postsynaptic density is involved in spine development and maturation.[12,45] To further validate the synaptic specificity of ISRIB treatment in FXS, we next examined *Fmr1* KO spine dynamics and the effect of ISRIB in normalizing changes elicited by FMRP deficiency. Overabundance of dendritic spines is a neuropathological hallmark of FXS and is a well-established phenotype in mouse models of FXS.[32,60–62] *In vivo* imaging has revealed that excess dendritic spines found on layer 1 apical dendrites of layer 5 pyramidal neurons in the cortex of adult *Fmr1* KO mice are a consequence of an overproduction and stabilization of spines during adolescence.[31] To measure spine dynamics, we treated mice with ISRIB or vehicle control for four days and measured the rate of spine formation and elimination by transcranial two-photon microscopy in layer 1 of the cortex. Spine formation was significantly increased in *Fmr1* KO mice compared to WT mice with vehicle treatment (p = 0.016, Mann-Whitney U). ISRIB treatment restored the rate of *Fmr1* KO spine formation to WT levels (WT + vehicle vs. *Fmr1* KO + ISRIB, p = 0.69, Mann-Whitney U). In contrast, the rate of spine elimination was not affected by FMRP deficiency and was unresponsive to ISRIB treatment (Figure 3; Table S3). This suggests an imbalance of spine stability in FXS that contributes to spine and synaptic changes in the disorder. Increased spine formation in FXS in conjunction with potential synaptic stabilization without a compensatory increase in spine elimination likely leads to the commonly observed phenotype of increased spine density in FXS.

ISRIB ameliorates social recognition deficits in *Fmr1* KO mice

Similar to individuals with FXS, adolescent *Fmr1* KO mice exhibit impaired social interaction behavior.[63] Proper social interaction involves complex coordinated neural network function, and subtle deficits in cortical network function and connectivity can manifest as observable

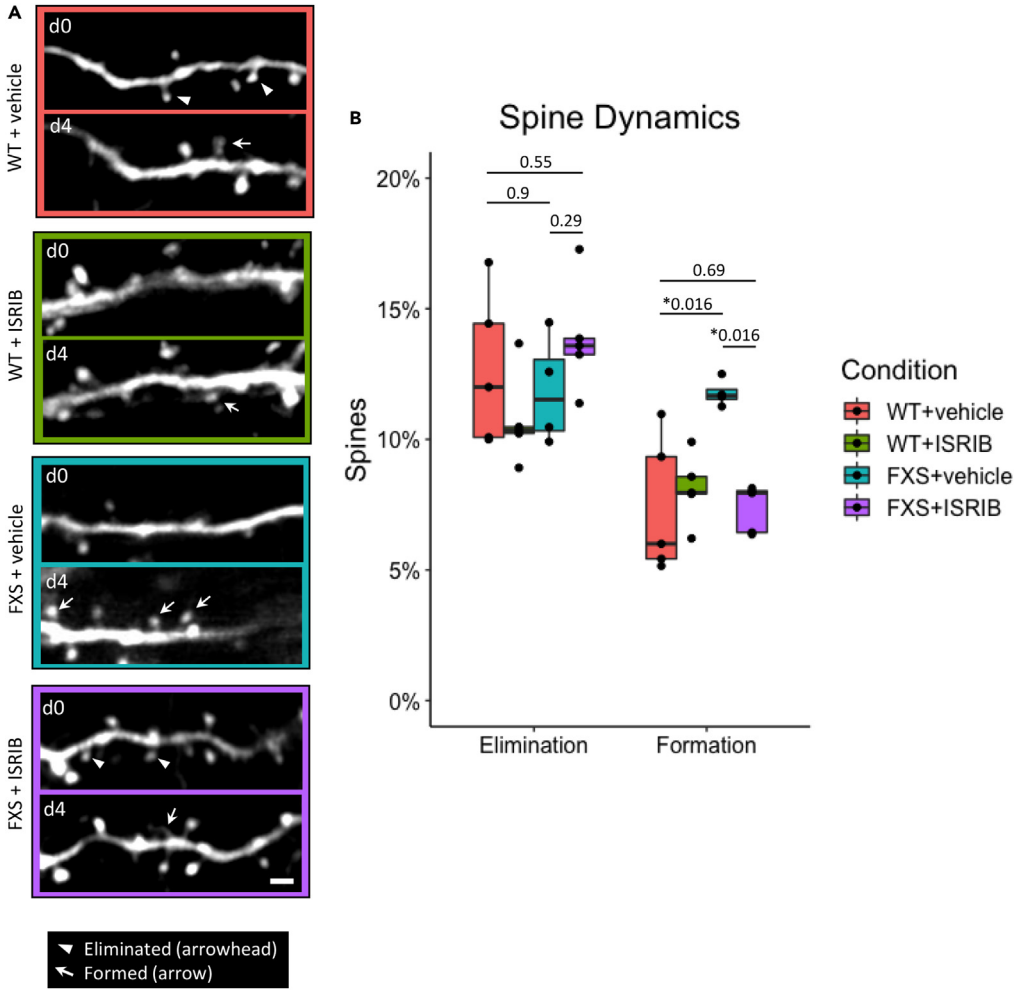

Figure 3. Transcranial two-photon imaging of dendritic spines in WT and *Fmr1* KO mice (FXS)

(A) Representative images of dendritic spines at day 0 (d0) and day 4 (d4) for each condition. Spine formation is indicated by arrows and spine elimination is indicated by arrowheads. Scale bar: 2 μm. Mice were treated with ISRIB or vehicle for four days and spines were imaged before (day 0) and after (day 4) treatment. Spine elimination and formation represents the change in spine count between day 0 and day 4.

(B) Quantification of dendritic spine elimination and formation. Vehicle-treated FXS mice exhibit an aberrantly high rate of spine formation compared to vehicle-treated WT mice (WT + vehicle vs. FXS + vehicle, p = 0.016). ISRIB treatment restored the rate of FXS spine formation to WT levels (WT + vehicle vs. FXS + ISRIB, p = 0.69). No deficits were observed in spine elimination. Significance was calculated by Mann-Whitney U test. FXS = *Fmr1* KO. n = 5 WT + vehicle, 5 WT + ISRIB, 4 FXS + vehicle, and 5 FXS + ISRIB. See also Table S3.

social interaction deficits. We thus sought to determine if the synaptic normalization we observed with ISRIB treatment is associated with improvements in behavioral outcomes. Using the three-chambered social novelty task, we asked whether ISRIB treatment improves social recognition in *Fmr1* KO mice (Figure 4A; Table S4). *Fmr1* KO mice displayed a significant deficit in social novelty preference, spending an equal amount of time interacting with a familiar mouse and a novel mouse (WT + vehicle vs. *Fmr1* KO + vehicle, p = 0.011, Mann-Whitney U).[64,65] ISRIB treatment increased social novelty preference in *Fmr1* KO mice, restoring preference to levels comparable to that of WT mice (*Fmr1* KO + vehicle vs. *Fmr1* KO + ISRIB, p = 0.019; WT + vehicle vs. *Fmr1* KO + ISRIB, p = 0.72, Mann-Whitney U). Conversely, WT and *Fmr1* KO vehicle and ISRIB-treated mice showed no difference in overall sociability (the preference to spend time with another mouse over an empty chamber) (Figure 4B; Table S5). Behavioral effects were not attributable to changes in locomotor behavior, as there was no significant difference in the total distance traveled in the arena (Figure S3; Table S6). Hyperactivity has been observed in *Fmr1* KO mice in previous studies,[66,67] however, after normalization for increased locomotion, social novelty and sociability outcomes were in line with our findings, suggesting that variability in anxiety levels does not affect social behavior. Additionally, some vehicles, including DMSO at high concentrations (32% and 64%), have been shown to affect locomotor activity in CD2F1 mice.[68] For behavioral testing, our vehicle contained only 5% DMSO and all mice received the vehicle. Locomotor activity is unlikely to be affected at this concentration but may be considered during interpretation. Overall, our results demonstrate that ISRIB treatment does rescue social recognition deficits in adolescent *Fmr1* KO mice.

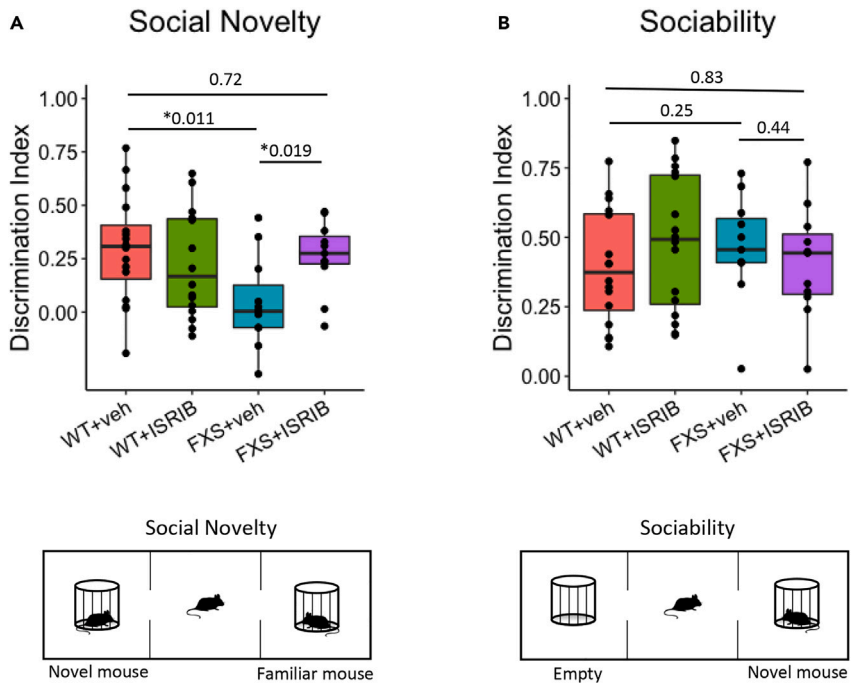

Figure 4. Behavioral analysis of *Fmr1* KO mice (FXS) with ISRIB treatment

(A) Social novelty was assessed using the three-chamber apparatus as diagrammed. One chamber houses a novel mouse, and the other chamber houses a familiar mouse. The amount of time spent investigating each mouse was quantified. The discrimination index is calculated as (novel interaction time - familiar interaction time)/(novel interaction time + familiar interaction time). FXS mice exhibit a deficit in social novelty preference compared to WT mice (WT + vehicle vs. FXS + vehicle, p = 0.011) and this effect is rescued by ISRIB treatment (FXS + vehicle vs. FXS + ISRIB, p = 0.019; WT + vehicle vs. FXS + ISRIB, p = 0.72). Significance was measured by Mann-Whitney U test. FXS = *Fmr1* KO. n = 16 WT + vehicle, 16 WT + ISRIB, 11 FXS + vehicle, and 11 FXS + ISRIB.

(B) Sociability was assessed using the three-chamber apparatus as diagrammed. One chamber houses an empty cage, and the other chamber houses a novel mouse. The amount of time spent investigating each cage was quantified and the discrimination index was calculated as described for social novelty. FXS mice showed no deficit in overall sociability (WT + vehicle vs. FXS + vehicle, p = 0.25). Significance was measured by Mann-Whitney U test. FXS = *Fmr1* KO. n = 16 WT + vehicle, 16 WT + ISRIB, 11 FXS + vehicle, and 11 FXS + ISRIB. See also Figure S3 and Tables S4–S6.

DISCUSSION

In this study, we investigated a mechanism for the development of dense, immature spines in FXS and examined the therapeutic potential of the translational regulator ISRIB in normalizing structural and molecular changes at the synapse. We demonstrated through population-level single synapse analysis that the loss of FMRP induces an unexpected shift toward increased synaptic PSD-95 and lower synaptic GluA1. This suggests a mechanism for the observation of increased density of spines with immature morphology in both individuals with FXS[61,62] and *Fmr1* KO mice.[66] Our data suggest that loss of the translational regulator FMRP leads to increased spine stabilization through elevated levels of PSD-95 at the synapse, thus increased density of spines and synapses; while also preventing further accumulation of glutamate receptors, which results in immature synaptic and spine development.

Interestingly, the overabundance of spines in FXS is developmentally regulated, observed early during postnatal week 1, normalized in adolescence from weeks 2–4, and re-emerging in adulthood.[29,43,44,69] Our study examined the developmental window in which spine abundance is normalized, thus we observed no defect in synaptic density in P26-P32 *Fmr1* KO cortex (Figure S4; Table S7). This apparent normalization belies developmental dynamics that will drive the nervous system toward aberrant connectivity. Our dendritic spine dynamics data are a window into this underlying developmental context. We show that FMRP loss corresponds with a decoupling of PSD-95 and GluA1 synaptic accumulation and a concomitant increase in the stabilization of new dendritic spines. The resulting large population of stabilized spines without a commensurate increase in elimination is likely the cause of the re-emergence of elevated immature spine density and synapses in the mature FXS brain. Thus, modulation of excessive spine formation with ISRIB treatment during this developmental window may mitigate the resulting overabundance of spines that emerges in adult *Fmr1* KO mice and improve cognitive and behavioral outcomes.

FMRP is a synaptic regulator of translation. Its function is controlled by synaptic activity, and it acts to regulate the translation of proteins involved in the development and maturation of spines and synapses.[2,7,12–16,19] In addition to its role in global translation, the role of FMRP on local synaptic translation is also critically important to synaptic plasticity and neuronal network function. FMRP regulates translational programs at each synapse to tune activity-dependent processes in neural plasticity.[11] This allows a neuron to modulate and prioritize its incoming information, thus effectively increasing the operational dynamic range of the nervous system. The loss of FMRP critically reduces the ability of

synapses to plastically respond to intercellular communication. A molecule that can restore, even partially, this synaptic control of translation could in theory compensate for some of the functions of FMRP and return the synaptic network to near normal function. We proposed that ISRIB, a stress-mediated translational modulator, might function as a compensatory mechanism in the absence of FMRP at the synapse.

ISRIB belongs to a class of small molecules that can modulate translation at the initiation phase, much like FMRP, and reduce the translation of specific classes of mRNAs.[70,71] Our study showed that ISRIB improves molecular accumulation of synaptic proteins, dendritic spine dynamics, and behavioral function in a mouse model of FXS. ISRIB improves social recognition memory, rescuing social novelty preference in *Fmr1* KO mice. Behavioral outcomes are a key functional measure of underlying improvements in molecular and cellular function, which often impact central regulatory pathways. Previously, ISRIB has been shown to improve cognitive function in brain injury,[72,73] cancer,[74] neuropsychiatric disorders,[75] neurodegenerative disorders,[25,76,77] and even healthy cognition.[70] Our study demonstrated the beneficial effects of ISRIB in a mouse model of FXS, which in combination with recent studies showing the impact of ISRIB treatment in models of Down syndrome[78] and MEHMO (mental retardation, epileptic seizures, hypogonadism and hypogenitalism, microcephaly, and obesity), a rare X-linked disorder,[79] expands its therapeutic potential to neurodevelopmental disorders. This broad efficacy of ISRIB treatment suggests a potentially shared framework of dysregulated translation across neurological diseases. We demonstrate that ISRIB rescues synaptic and behavioral phenotypes in FXS, highlighting the therapeutic potential of local synaptic protein regulation in alleviating the impact of FMRP deficiency in the brain.

Limitations of the study

We have shown previously that the cellular and synaptic changes observed in *Fmr1* KO cortex are layer and population specific and respond differentially to drug treatment.[29] In this study, we again demonstrated the layer and synapse-specific impact of FMRP loss and its pharmacological rescue. We showed that specific layer 1 synaptic deficits in *Fmr1* KO cortex respond to ISRIB treatment and can affect functional rescue in social recognition of *Fmr1* KO mice. While ISRIB decreases elevated PSD-95 levels and increases GluA1 levels in layer 1, PSD-95 levels are much less affected by both FMRP loss and ISRIB treatment in layer 2/3. The layer and population specific differences observed in this study as well as our previous study exemplify the heterogenous deficits and responses among synapses. Therefore, specific changes are not generalizable across all synapses and regions, and it is highly likely and expected that the behavioral outcomes described are dependent on the interplay between unique region-specific changes throughout the brain.

STAR★METHODS

Detailed methods are provided in the online version of this paper and include the following:

- KEY RESOURCES TABLE
- RESOURCE AVAILABILITY
  - Lead contact
  - Materials availability
  - Data and code availability
- EXPERIMENTAL MODEL AND STUDY PARTICIPANT DETAILS
- METHOD DETAILS
  - Drug treatment
  - Array tomography
  - Acute slice preparation
  - FUNCAT (fluorescent noncanonical amino acid tagging)
  - *In vivo* dendritic spine imaging
  - Three-chamber tests
- QUANTIFICATION AND STATISTICAL ANALYSIS

SUPPLEMENTAL INFORMATION

Supplemental information can be found online at https://doi.org/10.1016/j.isci.2024.109259.

ACKNOWLEDGMENTS

This work was supported by the National Institutes of Health F32 HD103451 (R.L.C.), F32 ES026872 (C.E.M.), K01 AG061230 (G.X.W.), R01 NS104950 (P.M. and Y.Z.), R01 MH109475 (Y.Z.), R01 AG071787 (Y.Z.), NICHD Autism Center of Excellence P50 HD109861 (P.M), FRAXA Research Foundation (R.L.C., G.X.W., and P.M.), John Merck Fund (G.X.W. and P.M.), Brain and Behavior Research Foundation (G.X.W.), Stanford University Mass Spectrometry seed grant (R.L.C.), and Stanford Psychiatry and Behavioral Sciences Trailblazing Trainee Award (R.L.C). P.W. is an HHMI investigator.

We thank Sabyn Nopar and Keerat Bains for help with animal husbandry, mouse perfusions, and necroscopies and Ana Radonovich for help with 3-chamber tests.

C.E.M. contributed to the project consistent with her previous role as a postdoctoral scholar at UCSC. The views and opinions expressed in this manuscript are those of the authors only and do not necessarily represent the views, official policy or position of the U.S. Department of Health and Human Services or any of its affiliated institutions or agencies.

AUTHOR CONTRIBUTIONS

R.L.C., C.E.M., J.H., P.W., P.M., Y.Z., and G.X.W. conceived and designed the project; R.L.C., V.F., C.E.M., and J.H. performed experiments and analyzed data; R.L.C., C.E.M., and G.X.W. wrote the paper; all authors edited and approved the paper.

DECLARATION OF INTERESTS

PW is an inventor on US Patent 9708247 held by the Regents of the University of California that describes ISRIB and its analogs. Rights to the invention have been licensed by UCSF to Calico.

Received: February 1, 2022
Revised: July 31, 2023
Accepted: February 13, 2024
Published: February 16, 2024

REFERENCES

1. Maenner, M.J., Shaw, K.A., Baio, J., Washington, A., Patrick, M., DiRienzo, M., Christensen, D.L., Wiggins, L.D., Pettygrove, S., Andrews, J.G., et al. (2020). Prevalence of Autism Spectrum Disorder Among Children Aged 8 Years — Autism and Developmental Disabilities Monitoring Network, 11 Sites, United States, 2016. MMWR. Surveill. Summ. *69*, 1–12. https://doi.org/10.15585/mmwr.mm6916a4.
2. Kelleher, R.J., and Bear, M.F. (2008). The Autistic Neuron: Troubled Translation? Cell *135*, 401–406. https://doi.org/10.1016/j.cell.2008.10.017.
3. Ey, E., Leblond, C.S., and Bourgeron, T. (2011). Behavioral profiles of mouse models for autism spectrum disorders. Autism Res. *4*, 5–16. https://doi.org/10.1002/aur.175.
4. Lozano, R., Rosero, C.A., and Hagerman, R.J. (2014). Fragile X spectrum disorders. Intractable Rare Dis. Res. *3*, 134–146. https://doi.org/10.5582/irdr.2014.01022.
5. Yamasue, H., Aran, A., and Berry-Kravis, E. (2019). Emerging pharmacological therapies in fragile X syndrome and autism. Curr. Opin. Neurol. *32*, 635–640. https://doi.org/10.1097/wco.0000000000000703.
6. O'Donnell, W.T., and Warren, S.T. (2002). A Decade of Molecular Studies of Fragile X Syndrome. Annu. Rev. Neurosci. *25*, 315–338. https://doi.org/10.1146/annurev.neuro.25.112701.142909.
7. Brown, V., Jin, P., Ceman, S., Darnell, J.C., O'donnell, W.T., Tenenbaum, S.A., Jin, X., Feng, Y., Wilkinson, K.D., Keene, J.D., et al. (2001). Microarray Identification of FMRP-Associated Brain mRNAs and Altered mRNA Translational Profiles in Fragile X Syndrome. Cell *107*, 477–487.
8. Feng, Y., Gutekunst, C.A., Eberhart, D.E., Yi, H., Warren, S.T., and Hersch, S.M. (1997). Fragile X mental retardation protein: Nucleocytoplasmic shuttling and association with somatodendritic ribosomes. J. Neurosci. *17*, 1539–1547. https://doi.org/10.1523/jneurosci.17-05-01539.1997.
9. Feng, Y., Absher, D., Eberhart, D.E., Brown, V., Malter, H.E., and Warren, S.T. (1997). FMRP associates with polyribosomes as an mRNP, and the I304N mutation of severe fragile X syndrome abolishes this association. Mol. Cell *1*, 109–118. https://doi.org/10.1016/S1097-2765(00)80012-X.
10. Dictenberg, J.B., Swanger, S.A., Antar, L.N., Singer, R.H., and Bassell, G.J. (2008). A Direct Role for FMRP in Activity-Dependent Dendritic mRNA Transport Links Filopodial-Spine Morphogenesis to Fragile X Syndrome. Dev. Cell *14*, 926–939. https://doi.org/10.1016/j.devcel.2008.04.003.
11. Weiler, I.J., Spangler, C.C., Klintsova, A.Y., Grossman, A.W., Kim, S.H., Bertaina-Anglade, V., Khaliq, H., De Vries, F.E., Lambers, F.A.E., Hatia, F., et al. (2004). Fragile X mental retardation protein is necessary for neurotransmitter- activated protein translation at synapses. Proc. Natl. Acad. Sci. USA *101*, 17504–17509. https://doi.org/10.1073/pnas.0407533101.
12. Bassell, G.J., and Warren, S.T. (2008). Fragile X Syndrome: Loss of Local mRNA Regulation Alters Synaptic Development and Function. Neuron *60*, 201–214. https://doi.org/10.1016/j.neuron.2008.10.004.
13. Darnell, J.C., Jensen, K.B., Jin, P., Brown, V., Warren, S.T., and Darnell, R.B. (2001). Fragile X mental retardation protein targets G quartet mRNAs important for neuronal function. Cell *107*, 489–499. https://doi.org/10.1016/S0092-8674(01)00566-9.
14. Miyashiro, K.Y., Beckel-Mitchener, A., Purk, T.P., Becker, K.G., Barret, T., Liu, L., Carbonetto, S., Weiler, I.J., Greenough, W.T., and Eberwine, J. (2003). RNA cargoes associating with FMRP reveal deficits in cellular functioning in Fmr1 null mice. Neuron *37*, 417–431. https://doi.org/10.1016/S0896-6273(03)00034-5.
15. Antar, L.N., Li, C., Zhang, H., Carroll, R.C., and Bassell, G.J. (2006). Local functions for FMRP in axon growth cone motility and activity-dependent regulation of filopodia and spine synapses. Mol. Cell. Neurosci. *32*, 37–48. https://doi.org/10.1016/j.mcn.2006.02.001.
16. Zalfa, F., Eleuteri, B., Dickson, K.S., Mercaldo, V., De Rubeis, S., Di Penta, A., Tabolacci, E., Chiurazzi, P., Neri, G., Grant, S.G.N., and Bagni, C. (2007). A new function for the fragile X mental retardation protein in regulation of PSD-95 mRNA stability. Nat. Neurosci. *10*, 578–587. https://doi.org/10.1038/nn1893.
17. Clarke, D.D., and Sokoloff, L. (1999). Circulation and Energy Metabolism of the Brain (Chemistry Faculty Publications), pp. 638–669.
18. Attwell, D., and Laughlin, S.B. (2001). An energy budget for signaling in the grey matter of the brain. J. Cerebr. Blood Flow Metabol. *21*, 1133–1145. https://doi.org/10.1097/00004647-200110000-00001.
19. Buffington, S.A., Huang, W., and Costa-Mattioli, M. (2014). Translational Control in Synaptic Plasticity and Cognitive Dysfunction. Annu. Rev. Neurosci. *37*, 17–38. https://doi.org/10.1146/annurev-neuro-071013-014100.
20. Davidovic, L., Navratil, V., Bonaccorso, C.M., Catania, M.V., Bardoni, B., and Dumas, M.E. (2011). A metabolomic and systems biology perspective on the brain of the Fragile X syndrome mouse model. Genome Res. *21*, 2190–2202. https://doi.org/10.1101/gr.116764.110.
21. El Bekay, R., Romero-Zerbo, Y., Decara, J., Sanchez-Salido, L., Del Arco-Herrera, I., Rodríguez-de Fonseca, F., and De Diego-Otero, Y. (2007). Enhanced markers of oxidative stress, altered antioxidants and NADPH-oxidase activation in brains from Fragile X mental retardation 1-deficient mice, a pathological model for Fragile X syndrome. Eur. J. Neurosci. *26*, 3169–3180. https://doi.org/10.1111/j.1460-9568.2007.05939.x.
22. Di Prisco, G.V., Huang, W., Buffington, S.A., Hsu, C.-C., Bonnen, P.E., Placzek, A.N., Sidrauski, C., Krnjević, K., Kaufman, R.J., Walter, P., and Costa-Mattioli, M. (2014). Translational control of mGluR-dependent long-term depression and object-place learning by eIF2α. Nat. Neurosci. *17*, 1073–1082. https://doi.org/10.1038/nn.3754.
23. Anand, A.A., and Walter, P. (2020). Structural insights into ISRIB, a memory-enhancing inhibitor of the integrated stress response. FEBS J. *287*, 239–245. https://doi.org/10.1111/febs.15073.
24. Rabouw, H.H., Langereis, M.A., Anand, A.A., Visser, L.J., De Groot, R.J., Walter, P., and Van Kuppeveld, F.J.M. (2019). Small molecule ISRIB suppresses the integrated stress response within a defined window of activation. Proc. Natl. Acad. Sci. USA *116*, 2097–2102. https://doi.org/10.1073/pnas.1815767116.
25. Wong, Y.L., Lebon, L., Edalji, R., Lim, H.B., Sun, C., and Sidrauski, C. (2018). The small

molecule ISRIB rescues the stability and activity of vanishing white matter disease eIF2B mutant complexes. Elife *7*, 1–23. https://doi.org/10.7554/eLife.32733.
26. Sidrauski, C., McGeachy, A.M., Ingolia, N.T., and Walter, P. (2015). The small molecule ISRIB reverses the effects of eIF2α phosphorylation on translation and stress granule assembly. Elife *4*, 1–16. https://doi.org/10.7554/eLife.05033.
27. Hooshmandi, M., Sharma, V., Thörn Perez, C., Sood, R., Krimbacher, K., Wong, C., Lister, K.C., Ureña Guzmán, A., Bartley, T.D., Rocha, C., et al. (2023). Excitatory neuron-specific suppression of the integrated stress response contributes to autism-related phenotypes in fragile X syndrome. Neuron *111*, 3028–3040.e6. https://doi.org/10.1016/j.neuron.2023.06.017.
28. Micheva, K.D., and Smith, S.J. (2007). Array Tomography: A New Tool for Imaging the Molecular Architecture and Ultrastructure of Neural Circuits. Neuron *55*, 25–36. https://doi.org/10.1016/j.neuron.2007.06.014.
29. Wang, G.X., Smith, S.J., and Mourrain, P. (2014). Fmr1 KO and Fenobam Treatment Differentially Impact Distinct Synapse Populations of Mouse Neocortex. Neuron *84*, 1273–1286. https://doi.org/10.1016/j.neuron.2014.11.016.
30. Wang, G.X., Smith, S.J., and Mourrain, P. (2016). Sub-synaptic, multiplexed analysis of proteins reveals fragile X related protein 2 is mislocalized in Fmr1 KO synapses. Elife *5*, e20560. https://doi.org/10.7554/eLife.20560.
31. Hodges, J.L., Yu, X., Gilmore, A., Bennett, H., Tjia, M., Perna, J.F., Chen, C.C., Li, X., Lu, J., and Zuo, Y. (2017). Astrocytic Contributions to Synaptic and Learning Abnormalities in a Mouse Model of Fragile X Syndrome. Biol. Psychiatr. *82*, 139–149. https://doi.org/10.1016/j.biopsych.2016.08.036.
32. Comery, T.A., Harris, J.B., Willems, P.J., Oostra, B.A., Irwin, S.A., Weiler, I.J., and Greenough, W.T. (1997). Abnormal dendritic spines in fragile X knockout mice: Maturation and pruning deficits. Proc. Natl. Acad. Sci. USA *94*, 5401–5404. https://doi.org/10.1073/PNAS.94.10.5401.
33. Irwin, S.A., Galvez, R., and Greenough, W.T. (2000). Dendritic spine structural anomalies in fragile-X mental retardation syndrome. Cerebr. Cortex *10*, 1038–1044. https://doi.org/10.1093/cercor/10.10.1038.
34. Grossman, A.W., Aldridge, G.M., Weiler, I.J., and Greenough, W.T. (2006). Local protein synthesis and spine morphogenesis: Fragile X syndrome and beyond. J. Neurosci. *26*, 7151–7155. https://doi.org/10.1523/JNEUROSCI.1790-06.2006.
35. Cane, M., Maco, B., Knott, G., and Holtmaat, A. (2014). The relationship between PSD-95 clustering and spine stability In Vivo. J. Neurosci. *34*, 2075–2086. https://doi.org/10.1523/JNEUROSCI.3353-13.2014.
36. Bats, C., Groc, L., and Choquet, D. (2007). The Interaction between Stargazin and PSD-95 Regulates AMPA Receptor Surface Trafficking. Neuron *53*, 719–734. https://doi.org/10.1016/j.neuron.2007.01.030.
37. De Roo, M., Klauser, P., Mendez, P., Poglia, L., and Muller, D. (2008). Activity-dependent PSD formation and stabilization of newly formed spines in hippocampal slice cultures. Cerebr. Cortex *18*, 151–161. https://doi.org/10.1093/cercor/bhm041.
38. Muddashetty, R.S., Nalavadi, V.C., Gross, C., Yao, X., Xing, L., Laur, O., Warren, S.T., and Bassell, G.J. (2011). Reversible Inhibition of PSD-95 mRNA Translation by miR-125a, FMRP Phosphorylation, and mGluR Signaling. Mol. Cell *42*, 673–688. https://doi.org/10.1016/j.molcel.2011.05.006.
39. Todd, P.K., Mack, K.J., and Malter, J.S. (2003). The fragile X mental retardation protein is required for type-I metabotropic glutamate receptor-dependent translation of PSD-95. Proc. Natl. Acad. Sci. USA *100*, 14374–14378. https://doi.org/10.1073/pnas.2336265100.
40. Harris, K.M., and Stevens, J.K. (1989). Dendritic spines of CA1 pyramidal cells in the rat hippocampus: Serial electron microscopy with reference to their biophysical characteristics. J. Neurosci. *9*, 2982–2997. https://doi.org/10.1523/jneurosci.09-08-02982.1989.
41. Matt, L., Kim, K., Hergarden, A.C., Patriarchi, T., Malik, Z.A., Park, D.K., Chowdhury, D., Buonarati, O.R., Henderson, P.B., Gökçek Saraç, Ç., et al. (2018). α-Actinin Anchors PSD-95 at Postsynaptic Sites. Neuron *97*, 1094–1109.e9. https://doi.org/10.1016/j.neuron.2018.01.036.
42. Kuriu, T., Inoue, A., Bito, H., Sobue, K., and Okabe, S. (2006). Differential control of postsynaptic density scaffolds via actin-dependent and -independent mechanisms. J. Neurosci. *26*, 7693–7706. https://doi.org/10.1523/JNEUROSCI.0522-06.2006.
43. Nimchinsky, E. a, Oberlander, a M., and Svoboda, K. (2001). Abnormal development of dendritic spines in FMR1 knock-out mice. J. Neurosci. *21*, 5139–5146.
44. Galvez, R., and Greenough, W.T. (2005). Sequence of abnormal dendritic spine development in primary somatosensory cortex of a mouse model of the fragile X mental retardation syndrome. Am. J. Med. Genet. *135*, 155–160. https://doi.org/10.1002/ajmg.a.30709.
45. El-Husseini, A.E., Schnell, E., Chetkovich, D.M., Nicoll, R.A., and Bredt, D.S. (2000). PSD-95 involvement in maturation of excitatory synapses. Science *290*, 1364–1368. https://doi.org/10.1126/science.290.5495.1364.
46. Stein, V., House, D.R.C., Bredt, D.S., and Nicoll, R.A. (2003). Postsynaptic density-95 mimics and occludes hippocampal long-term potentiation and enhances long-term depression. J. Neurosci. *23*, 5503–5506. https://doi.org/10.1523/jneurosci.23-13-05503.2003.
47. Ehrlich, I., and Malinow, R. (2004). Postsynaptic Density 95 controls AMPA Receptor Incorporation during Long-Term Potentiation and Experience-Driven Synaptic Plasticity. J. Neurosci. *24*, 916–927. https://doi.org/10.1523/JNEUROSCI.4733-03.2004.
48. Suresh, A., and Dunaevsky, A. (2017). Relationship between synaptic AMPAR and spine dynamics: Impairments in the FXS mouse. Cerebr. Cortex *27*, 4244–4256. https://doi.org/10.1093/cercor/bhx128.
49. Aryal, S., and Klann, E. (2018). Turning up translation in fragile X syndrome. Science *361*, 648–649. https://doi.org/10.1126/science.aau6450.
50. Dionne, O., Lortie, A., Gagnon, F., and Corbin, F. (2021). Rates of protein synthesis are reduced in peripheral blood mononuclear cells (PBMCs) from fragile X individuals. PLoS One *16*, e0251367. https://doi.org/10.1371/journal.pone.0251367.
51. Qin, M., Kang, J., Burlin, T.V., Jiang, C., and Smith, C.B. (2005). Postadolescent changes in regional cerebral protein synthesis: An in vivo study in the Fmr1 null mouse. J. Neurosci. *25*, 5087–5095. https://doi.org/10.1523/JNEUROSCI.0093-05.2005.
52. Qin, M., Schmidt, K.C., Zametkin, A.J., Bishu, S., Horowitz, L.M., Burlin, T.V., Xia, Z., Huang, T., Quezado, Z.M., and Smith, C.B. (2013). Altered cerebral protein synthesis in fragile X syndrome: Studies in human subjects and knockout mice. J. Cerebr. Blood Flow Metabol. *33*, 499–507. https://doi.org/10.1038/jcbfm.2012.205.
53. Donnard, E., Shu, H., and Garber, M. (2022). Single cell transcriptomics reveals dysregulated cellular and molecular networks in a fragile X syndrome model. PLoS Genet. *18*, e1010221–e1010225. https://doi.org/10.1371/journal.pgen.1010221.
54. Jacquemont, S., Pacini, L., Jønch, A.E., Cencelli, G., Rozenberg, I., He, Y., D'Andrea, L., Pedini, G., Eldeeb, M., Willemsen, R., et al. (2018). Protein synthesis levels are increased in a subset of individuals with fragile X syndrome. Hum. Mol. Genet. *27*, 2039–2051. https://doi.org/10.1093/hmg/ddy099.
55. Osterweil, E.K., Krueger, D.D., Reinhold, K., and Bear, M.F. (2010). Hypersensitivity to mGluR5 and ERK1/2 leads to excessive protein synthesis in the hippocampus of a mouse model of fragile X syndrome. J. Neurosci. *30*, 15616–15627. https://doi.org/10.1523/JNEUROSCI.3888-10.2010.
56. Ceolin, L., Bouquier, N., Vitre-Boubaker, J., Rialle, S., Severac, D., Valjent, E., Perroy, J., and Puighermanal, E. (2017). Cell type-specific mRNA dysregulation in hippocampal CA1 pyramidal neurons of the fragile X syndrome mouse model. Front. Mol. Neurosci. *10*, 1–11. https://doi.org/10.3389/fnmol.2017.00340.
57. Thomson, S.R., Seo, S.S., Barnes, S.A., Louros, S.R., Muscas, M., Dando, O., Kirby, C., Wyllie, D.J.A., Hardingham, G.E., Kind, P.C., and Osterweil, E.K. (2017). Cell-Type-Specific Translation Profiling Reveals a Novel Strategy for Treating Fragile X Syndrome. Neuron *95*, 550–563.e5. https://doi.org/10.1016/j.neuron.2017.07.013.
58. Greenblatt, E.J., and Spradling, A.C. (2018). Fragile X mental retardation 1 gene enhances the translation of large autism-related proteins. Science *361*, 709–712. https://doi.org/10.1126/science.aas9963.
59. Seo, S.S., Louros, S.R., Anstey, N., Gonzalez-Lozano, M.A., Harper, C.B., Verity, N.C., Dando, O., Thomson, S.R., Darnell, J.C., Kind, P.C., et al. (2022). Excess ribosomal protein production unbalances translation in a model of Fragile X Syndrome. Nat. Commun. *13*, 3236. https://doi.org/10.1038/s41467-022-30979-0.
60. Bagni, C., and Greenough, W.T. (2005). From mRNP trafficking to spine dysmorphogenesis: The roots of fragile X syndrome. Nat. Rev. Neurosci. *6*, 376–387. https://doi.org/10.1038/nrn1667.
61. Rudelli, R.D., Brown, W.T., Wisniewski, K., Jenkins, E.C., Laure-Kamionowska, M., Connell, F., and Wisniewski, H.M. (1985). Adult fragile X syndrome - Clinico-neuropathologic findings. Acta Neuropathol. *67*, 289–295. https://doi.org/10.1007/BF00687814.
62. Hinton, V.J., Brown, W.T., Wisniewski, K., and Rudelli, R.D. (1991). Analysis of neocortex in three males with the fragile X syndrome. Am. J. Med. Genet. *41*, 289–294. https://doi.org/10.1002/ajmg.1320410306.
63. Kazdoba, T.M., Leach, P.T., Silverman, J.L., and Crawley, J.N. (2014). Modeling fragile X syndrome in the Fmr1 knockout mouse.

Intractable Rare Dis. Res. *3*, 118–133. https://doi.org/10.5582/irdr.2014.01024.

64. McNaughton, C.H., Moon, J., Strawderman, M.S., Maclean, K.N., Evans, J., and Strupp, B.J. (2008). Evidence for Social Anxiety and Impaired Social Cognition in a Mouse Model of Fragile X Syndrome. Behav. Neurosci. *122*, 293–300. https://doi.org/10.1037/0735-7044.122.2.293.
65. Dahlhaus, R., and El-Husseini, A. (2010). Altered neuroligin expression is involved in social deficits in a mouse model of the fragile X syndrome. Behav. Brain Res. *208*, 96–105. https://doi.org/10.1016/j.bbr.2009.11.019.
66. Consortium, T.D.-G.F.X. (1994). Fmr1 knockout mice: a model to study fragile X mental retardation. Cell *78*, 23–33.
67. Sørensen, E.M., Bertelsen, F., Weikop, P., Skovborg, M.M., Banke, T., Drasbek, K.R., and Scheel-Krüger, J. (2015). Hyperactivity and lack of social discrimination in the adolescent Fmr1 knockout mouse. Behav. Pharmacol. *26*, 733–740. https://doi.org/10.1097/FBP.0000000000000152.
68. Castro, C.A., Hogan, J.B., Benson, K.A., Shehata, C.W., and Landauer, M.R. (1995). Behavioral effects of vehicles: DMSO, ethanol, Tween-20, Tween-80, and emulphor-620. Pharmacol. Biochem. Behav. *50*, 521–526. https://doi.org/10.1016/0091-3057(94)00331-9.
69. He, C.X., and Portera-Cailliau, C. (2013). The trouble with spines in fragile X syndrome: Density, maturity and plasticity. Neuroscience *251*, 120–128. https://doi.org/10.1016/j.neuroscience.2012.03.049.
70. Sidrauski, C., Acosta-Alvear, D., Khoutorsky, A., Vedantham, P., Hearn, B.R., Li, H., Gamache, K., Gallagher, C.M., Ang, K.K.H., Wilson, C., et al. (2013). Pharmacological brake-release of mRNA translation enhances cognitive memory. Elife *2*, e00498. https://doi.org/10.7554/eLife.00498.
71. Tsai, J.C., Miller-Vedam, L.E., Anand, A.A., Jaishankar, P., Nguyen, H.C., Renslo, A.R., Frost, A., and Walter, P. (2018). Structure of the nucleotide exchange factor eIF2B reveals mechanism of memory-enhancing molecule. Science *359*, eaaq0939. https://doi.org/10.1126/science.aaq0939.
72. Chou, A., Krukowski, K., Jopson, T., Zhu, P.J., Costa-Mattioli, M., Walter, P., and Rosi, S. (2017). Inhibition of the integrated stress response reverses cognitive deficits after traumatic brain injury. Proc. Natl. Acad. Sci. USA *114*, E6420–E6426. https://doi.org/10.1073/pnas.1707661114.
73. Chang, L., Liu, X., Chen, J., Liu, H., Wang, G., Wang, G., Liao, X., and Shen, X. (2022). Attenuation of Activated eIF2α Signaling by ISRIB Treatment After Spinal Cord Injury Improves Locomotor Function. J. Mol. Neurosci. *72*, 585–597. https://doi.org/10.1007/s12031-021-01920-9.
74. Lorenz, N.I., Sittig, A.C.M., Urban, H., Luger, A.L., Engel, A.L., Münch, C., Steinbach, J.P., and Ronellenfitsch, M.W. (2021). Activating transcription factor 4 mediates adaptation of human glioblastoma cells to hypoxia and temozolomide. Sci. Rep. *11*, 14161. https://doi.org/10.1038/s41598-021-93663-1.
75. Kabir, Z.D., Che, A., Fischer, D.K., Rice, R.C., Rizzo, B.K., Byrne, M., Glass, M.J., De Marco Garcia, N.V., and Rajadhyaksha, A.M. (2017). Rescue of impaired sociability and anxiety-like behavior in adult cacna1c-deficient mice by pharmacologically targeting eIF2α. Mol. Psychiatr. *22*, 1096–1109. https://doi.org/10.1038/mp.2017.124.
76. Xu, H., Bensalel, J., Capobianco, E., Lu, M.L., and Wei, J. (2022). Impaired Restoration of Global Protein Synthesis Contributes to Increased Vulnerability to Acute ER Stress Recovery in Huntington's Disease. Cell. Mol. Neurobiol. *42*, 2757–2771. https://doi.org/10.1007/s10571-021-01137-9.
77. Oliveira, M.M., Lourenco, M.V., Longo, F., Kasica, N.P., Yang, W., Ureta, G., Ferreira, D.D.P., Mendonça, P.H.J., Bernales, S., Ma, T., et al. (2021). Correction of eIF2-dependent defects in brain protein synthesis, synaptic plasticity, and memory in mouse models of Alzheimer's disease. Sci. Signal. *14*, eabc5429–12. https://doi.org/10.1126/scisignal.abc5429.
78. Zhu, P.J., Khatiwada, S., Cui, Y., Reineke, L.C., Dooling, S.W., Kim, J.J., Li, W., Walter, P., and Costa-Mattioli, M. (2019). Activation of the ISR mediates the behavioral and neurophysiological abnormalities in down syndrome. Science *366*, 843–849. https://doi.org/10.1126/science.aaw5185.
79. Young-Baird, S.K., Lourenço, M.B., Elder, M.K., Klann, E., Liebau, S., and Dever, T.E. (2020). Suppression of MEHMO Syndrome Mutation in eIF2 by Small Molecule ISRIB. Mol. Cell *77*, 875–886.e7. https://doi.org/10.1016/j.molcel.2019.11.008.
80. Allen, N.J., Bennett, M.L., Foo, L.C., Wang, G.X., Chakraborty, C., Smith, S.J., and Barres, B.A. (2012). Astrocyte glypicans 4 and 6 promote formation of excitatory synapses via GluA1 AMPA receptors. Nature *486*, 410–414. https://doi.org/10.1038/nature11059.
81. Hiu, T., Farzampour, Z., Paz, J.T., Wang, E.H.J., Badgely, C., Olson, A., Micheva, K.D., Wang, G., Lemmens, R., Tran, K.V., et al. (2016). Enhanced phasic GABA inhibition during the repair phase of stroke: A novel therapeutic target. Brain *139*, 468–480. https://doi.org/10.1093/brain/awv360.
82. Kaidanovich-Beilin, O., Lipina, T., Vukobradovic, I., Roder, J., and Woodgett, J.R. (2011). Assessment of Social Interaction Behaviors. J. Vis. Exp. *0*, 2473–2476. https://doi.org/10.3791/2473.
83. Friard, O., and Gamba, M. (2016). BORIS: a free, versatile open-source event-logging software for video/audio coding and live observations. Methods Ecol. Evol. *7*, 1325–1330. https://doi.org/10.1111/2041-210X.12584.

STAR★METHODS

KEY RESOURCES TABLE

REAGENT or RESOURCE	SOURCE	IDENTIFIER
Antibodies		
GluA1	Millipore	Cat# AB1504; RRID: AB_2113602
VGlut2	Millipore	Cat# AB2251; RRID: AB_1587626
PSD-95	Cell Signaling	Cat# 3450; RRID: AB_2292883
VGlut1	Millipore	Cat# AB5905; RRID: AB_2301751
Synapsin-1	Cell Signaling	Cat# 5297; RRID: AB_2616578
Goat anti-Mouse Alexa 594	Invitrogen	Cat# A110032
Goat anti-Guinea Pig Alexa 594	Invitrogen	Cat# A11076
Goat anti-Mouse Alexa 488	Invitrogen	Cat# A11029
Goat anti-Rabbit Alexa 594	Invitrogen	Cat# A11034
Goat anti-Rabbit Alexa 647	Invitrogen	Cat# A21245
Chemicals, peptides, and recombinant proteins		
ISRIB	Millipore Sigma	Cat# 50-958-40001
L-Homopropargylglycine (HPG)	Vector Laboratories	Cat# CCT-1067
Alexa Fluor 647 Azide	Invitrogen	Cat# A10277
Experimental models: Organisms/strains		
B6.129P2-*Fmr1*^{tm1Cgr}/J (backcrossed to C57BL/6J)	Stephen Warren, Emory University	Strain # 003025
B6.Cg-Tg(Thy1-YFP)HJrs/J (backcrossed to C57BL/6J)	The Jackson Laboratory	Strain # 003782

RESOURCE AVAILABILITY

Lead contact

Further information and requests for resources and reagents should be directed to and will be fulfilled by the lead contact, Gordon X. Wang (gordon.wang@stanford.edu).

Materials availability

This study did not generate new unique reagents.

Data and code availability

- Data: All data reported in this paper will be shared by the lead contact upon request.
- Code: This paper does not report original code.
- Any additional information required to reanalyze the data reported in this paper is available from the lead contact upon request.

EXPERIMENTAL MODEL AND STUDY PARTICIPANT DETAILS

The Institutional Animal Care and Use Committee of University of California Santa Cruz approved all animal care and experimental procedures. Mice were group housed under a 12-h light-dark cycle with *ad libitum* food and water. The *Fmr1* KO mice were a gift from Dr. Stephen T. Warren at Emory University. Thy1-YFP-H transgenic mice (stock number 003782), used for dendritic spine experiments were purchased from The Jackson Laboratory (Bar Harbor, ME). All mice were backcrossed with C57BL/6J mice more than 10 generations to produce congenic strains. Males (*Fmr1* KO and WT littermates) were used in all experiments. Experiments were conducted on adolescent mice, age P26-P32 for all experiments except FUNCAT (P27-P37).

METHOD DETAILS

Drug treatment

Animals received ISRIB at 2.5 mg/kg in 50% DMSO and 50% PEG400 for two-photon microscopy or 1 mg/kg in 5% DMSO, 2% Polysorbate 80, 20% PEG400, and 73% dextrose water for array tomography and behavioral testing, or a matched volume of the appropriate vehicle once per day by intraperitoneal injection. Mice were treated for 4 days for array tomography and two-photon imaging and 2 days for behavioral testing.

Array tomography

Tissue and ribbon array preparation, immunohistochemistry, and microscopy were performed as described previously,[28] and outlined below.

Tissue and ribbon array preparation

Mice were perfused with 4% paraformaldehyde and brains were removed. A small piece of tissue (~2 mm deep x 1 mm wide x 1 mm long) was cut from the motor cortex of WT and *Fmr1* KO males age P26-P32. Tissue was dehydrated in 50%, 70%, 95%, and 100% ethanol, then embedded in LRWhite resin (hard grade) in gelatin capsules. Sections of 70 nm were cut using an ultramicrotome, creating a ribbon array of serial sections, which was placed on a gelatin-coated coverslip. Tissues were paired so that each coverslip contained two ribbons, one of each genotype for a given treatment (vehicle or ISRIB), to minimize slide to slide variability.

Immunohistochemistry

For immunostaining, coverslips containing ribbon arrays were washed in Tris buffer (Tris/50 mM glycine/0.05% Tween) and primary antibodies were applied in Tris buffer containing 0.1% BSA. Coverslips containing antibodies were incubated at 4°C overnight in a humidified chamber. Coverslips were washed in Tris buffer 3 × 5 min and secondary antibodies were applied in Tris buffer containing 0.1% BSA for 30 min at room temperature. Coverslips were washed with Tris buffer 3 × 5 min, rinsed with milliQ H_2O, and mounted in SlowFade Gold anti-fade with DAPI (Invitrogen). After imaging, mounting media was washed with milliQ H_2O and antibodies were eluted with 0.2M NaOH/0.02% SDS for 5 min. The next round of staining was performed immediately after elution or coverslip was allowed to dry completely.

Microscopy

Ribbons were imaged on a Zeiss Axio Imager.Z1 Upright Fluorescence Microscope with a motorized stage and Axiocam HR Digital Camera. The same field of view for each Layer 1 and Layer 2/3 cortical region were imaged for every section within each array and for every round of staining. Images were taken using a Zeiss 63x/1.4 NA Plan Apochromat objective with the same exposure for both ribbons on each coverslip. All microscopy was performed blinded to genotype and treatment.

Image processing

Image stacks were imported into FIJI and registered across all image sessions using a rigid model with interpolation. Registered images were deconvolved in MATLAB using the Richardson-Lucy technique with background subtraction and an empirical point spread function (PSF) through ten iterations. Empirical PSF were measured using the actual imaging system with 110 nm beads mounted on slides. Images were aligned with TrakEM in FIJI by both rigid least squares (linear feature correspondences) and elastic (non-linear block correspondences) alignments.

Synapse classification

Synapse classification is based on a set of requirements, as described previously.[29,80,81] Utilizing specific protein localization profiles for each synaptic population, established by Wang et al., 2016, synapses are identified and classified using three points: the origin (PSD-95), the terminus (Synapsin), and a third marker with a defined pre- or post-synaptic distance (VGlut1 or VGlut2).[30] A vector is drawn between the centers of mass from origin to terminus, defining a colocaliztion sphere centered around the origin. A third marker, such as VGlut1 or VGlut2 must fall within this sphere. Distances to the pre- and post-synaptic marker are utilized to confirm potential synapses identified by this PSD-95/Synapsin colocalization and provide more specificity in synapse type. For a presynaptic marker, the synapse is verified if the distance to Synapsin is smaller than the distance to PSD-95, otherwise, the potential synaptic axis is removed. If more than one-third point falls within a colocalization sphere, the dataset is checked for overlapping spheres and points are assigned to maximize verified synapses. If a single third point is shared between two spheres, it is assigned to the synapse with the shortest pre- or post-synaptic distance as previously defined. Synaptic density is calculated as the total number of cortical-cortical excitatory synapses per non-nuclear volume of tissue.

Synaptic protein analysis

Signal volume represents the number of voxels per puncta. Volume was used as a measure of PSD-95 abundance and postsynaptic size for each individual synapse, and the distribution was plotted as a cumulative distribution function and density curve. Significant shifts in distribution were tested by Kolmogorov-Smirnov and significant differences in median volume were tested by Mann-Whitney U. Integrated intensity was used as a measure of GluA1 abundance. GluA1 abundance is a weighted average of VGlut1 and VGlut2 synapses based on their relative contribution to the excitatory synapse population (L1: 89.144% VGlut1, 10.856% VGlut2; L2/3: 85.008% VGlut1, 14.992% VGlut2). The ratio of ISRIB/vehicle was calculated for each pair of tissue imaged at the same time for each genotype. Significant differences were tested by Mann-Whitney U.

Normalization

All tissues were processed in pairs (fix, dissect, embed, section, and stain). Exposure levels and segmentation thresholds were set with identical parameters based on previously validated methods. The pairing of animals and tissues allows us to reduce variability and minimize animal

use. For ratio analyses (e.g., ISRIB/vehicle), pair information is maintained, and direct comparisons are made. When pairs are mixed (e.g., distribution curves), normalization of the entire distribution is performed on a per animal basis based on each animal's maximum observed value, correcting for shifts in distribution bounds.

Acute slice preparation

Male *Fmr1* KO and WT mice (P27-P37) were anesthetized with isoflurane and decapitated. The brain was quickly removed and submerged in ice-cold oxygenated ACSF (125 mM NaCl, 2.5 mM KCl, 25 mM $NaHCO_3$, 1.25 mM NaH_2PO_4, 25 mM glucose, 3 mM $MgCl_2$, 0.1 mM $CaCl_2$). Brains were sliced on a vibratome (Leica) into 400 μm sections and slices were transferred to 32°C oxygenated ACSF supplemented with sucrose (ACSF, 30 mM sucrose, 2 mM $MgCl_2$, 1 mM $CaCl_2$) and left to recover for 1 h. After recovery, slices were transferred to 32°C oxygenated Ringer's solution (ACSF, 1 mM $MgCl_2$, 2 mM $CaCl_2$) for FUNCAT.

FUNCAT (fluorescent noncanonical amino acid tagging)

Slices were treated with 200 mM ISRIB or DMSO for 1 h in 32°C oxygenated Ringer's solution. 4 mM HPG or methionine was added, and slices were incubated for 2 h for metabolic labeling. Slices were then washed briefly with PBS-MC (1 mM $MgCl_2$, 0.1 mM $CaCl_2$) and fixed in 4% formaldehyde/4% sucrose for 20 min at room temperature. Slices were washed again with PBS-MC, then transferred to 30% sucrose at 4°C until slices sunk to the bottom of the dish. Slices were then frozen in blocks of 30% sucrose and sliced to 50 μm on a microtome (Leica). Slices were permeabilized (0.5% Triton X-100, 10% normal horse serum, 5% sucrose, 2% bovine serum albumin in PBS), shaking gently overnight at room temperature. Slices were washed three times with 0.1% Triton X-100 in PBS and the FUNCAT reaction mixture was added (1.25 mM THPTA, 2.5 mM sodium ascorbate, 2 μM Alexa Fluor 647 azide (Thermo Fisher), 250 μM $CuSO_4$ in PBS) and the reaction was incubated overnight at room temperature with gentle shaking. Slices were washed 3 × 20 min at room temperature (0.5 mM EDTA, 1% Tween 20 in PBS), then in PBS/0.1% Tween 20. 5 μg/mL DAPI was added to slices in PBS and slices were mounted with ProLong Diamond Antifade Mountant (Thermo Fisher). Slices were imaged on a Zeiss LSM980 inverted confocal microscope. z stack images were acquired with a Zeiss 25× oil objective using Nyquist settings. Stacked images were sum projected and layer 1 and layer 2/3 were segmented as separate ROIs for analysis. ROIs were segmented based on DAPI and fluorescence intensity was measured for cell bodies as a halo around each nucleus. All images were normalized for background fluorescence and HPG-labeled slices were normalized to methionine controls. Individual cell measurements were averaged and reported for each sample.

In vivo dendritic spine imaging

Transcranial two-photon imaging of dendritic spines and data analysis were conducted as described previously.[31] Tg(Thy1-YFP)H were crossed into the *Fmr1* KO line to produce a line expressing YFP within the apical dendrites and spines of motor cortex layer 5 neurons, making them amenable to transcranial two-photon imaging of spine dynamics. P26-P32 YFP-expressing WT and *Fmr1* KO males were used for *in vivo* two-photon imaging experiments. Collected image stacks were analyzed using ImageJ. Mice received daily vehicle or ISRIB treatment for 4 days between the day 0 and day 4 imaging sessions. The percentage of eliminated and formed spines was calculated as the difference in the number of spines between the day 0 and day 4 imaging sessions divided by the number of spines counted for the day 0 imaging session. Mann-Whitney U test was used to determine differences in spine dynamics.

Three-chamber tests

The same general testing protocol was used to evaluate both sociability and social novelty in vehicle and ISRIB-treated P26-P32 *Fmr1* KO mice and WT littermates. The test apparatus consists of three chambers (20 × 40 × 20 cm each) with openings to enable free access to each chamber.[82] The two side chambers contain cylindrical wire cages as confinements for novel and familiar age-matched, same sex probe mice. First, the mice were allowed to freely explore all three chambers for 10 min without any additional mice present in the wire enclosures. During the sociability test phase, an unfamiliar C57BL/6J mouse was put inside one wire cage while the other wire cage remained empty. During the social novelty test phase, an unfamiliar male C57BL/6J mouse was placed in one wire cage, while the other wire cage contained a familiar mouse. During both testing phases, the subject mice were allowed to freely explore all chambers for 10 min. Chambers and cages were cleaned with 70% ethanol between each testing session. Mice were video recorded and the duration of time each mouse spent investigating each wire cage was quantified using Behavioral Observation Research Interactive Software (BORIS v. 7.10.2).[83] Interaction is determined when the mouse is close to and facing the wired cage. Behaviors were annotated manually, and analysis was performed blind to genotype. Assessment of general locomotion was carried out by measuring the total distance traveled by each mouse during habituation and testing. Changes in social novelty, sociability, and locomotion were tested by Mann-Whitney U test.

QUANTIFICATION AND STATISTICAL ANALYSIS

Significance was measured by Mann-Whitney U, which does not require the data to conform to the normal distribution assumptions of parametric tests. We have represented the distribution of our data as much as possible in each plot (e.g., density plots, boxplots with individual points) to provide a more transparent display of the data and its distribution.